A&A 403, 1175–1184 (2003)
DOI: 10.1051/0004-6361:20030405


Astronomy & Astrophysics

# A complete set of radiative and Auger rates for K-vacancy states in Fe XVIII–Fe XXV⋆

P. Palmeri[1,⋆⋆], C. Mendoza[1,⋆⋆⋆], T. R. Kallman[1], and M. A. Bautista[2]

[1] NASA Goddard Space Flight Center, Code 662, Greenbelt, MD 20771, USA
[2] Centro de Física, Instituto Venezolano de Investigaciones Científicas (IVIC), PO Box 21827, Caracas 1020A, Venezuela

Received 26 November 2002 / Accepted 17 March 2003

**Abstract.** A complete set of level energies, wavelengths, *A*-values, and total and partial Auger rates have been computed for transitions involving the K-vacancy states within the $n = 2$ complex of Fe XVIII–Fe XXV. Three different standard numerical packages are used for this purpose, namely AUTOSTRUCTURE, the Breit–Pauli *R*-matrix suite (BPRM) and HFR, which allow reliable estimates of the physical effects involved and of the accuracy of the resulting data sets. The Breit interaction is taken into account because its contributions to the small *A*-values and partial Auger rates cannot be neglected with increasing electron occupancy. Semiempirical adjustments can also lead to large differences in both the radiative and Auger decay data of strongly mixed levels. Several experimental level energies and wavelengths are questioned, and significant discrepancies are found with previously computed decay rates that are attributed to numerical problems. The statistical accuracy of the present level energies and wavelengths is ranked at ±3 eV and ±2 mÅ, respectively, and that for *A*-values and partial Auger rates greater than $10^{13}$ s$^{-1}$ at better than 20%.

**Key words.** atomic data – atomic processes – X-rays: general

## 1. Introduction

We are currently involved in a project to calculate accurate atomic data for the modeling of iron K lines. It has been motivated by the diagnostic potential of these lines in the X-ray spectra of high energy environments (quasars, active galactic nuclei, galactic black-hole candidates) that are being focused now by powerful satellite-borne telescopes (*Chandra*, *XMM-Newton*), and will gain greater importance with the launch of the *Astro-E2* telescope. In an earlier report on the decay properties of the K-vacancy states in Fe XXIV (Bautista et al. 2003), to be referred to hereafter as Paper I, a numerical approach was established that led to data sets of *A*-values and Auger rates with a suggested accuracy of 10–15%. It relies on calculations with several general-use computational atomic physics codes and extensive comparisons with previous work. A formal treatment of the Breit interaction was emphasized then in the case of the distinctively magnetic Fe Li-like ion, leading to critical evaluations of the effectiveness of the different computational packages in the treatment of inner-shell processes and of the quality of previously available data.

*Send offprint requests to*: T. R. Kallman,
e-mail: timothy.r.kallman@nasa.gov

⋆ Tables 1, 2 and 8 are only available in electronic form at http://www.edpsciences.org

⋆⋆ Research Associate, Department of Astronomy, University of Maryland, College Park, MD 20742.
⋆⋆⋆ *Present address:* Centro de Física, IVIC, Caracas 1020A.

The approach of Paper I is here extended to generate a complete set of energy levels, wavelengths, *A*-values and Auger rates for all the K-vacancy states of the $n = 2$ complex in Fe XVIII–Fe XXV. In this respect, the critical compilation by Shirai et al. (2000) certifies the current incompleteness of the inner-shell level structures of Fe ions which is a major obstacle in line identification and spectral modeling in the above mentioned astrophysical endeavors. Although the precision of computed wavelengths does not match that of measurements by an order of magnitude, as shown in Paper I, an exhaustive and reasonably accurate (~1 mÅ, say) inventory will certainly facilitate spectroscopic identifications, be an asset in the resolution of line blends and lead to further structural refinement. A survey of the radiative and autoionization data for Fe ions with electron occupancies $N \leq 6$ computed by Chen (1986), Chen & Crasemann (1987, 1988), Chen et al. (1997) and those contained in the "Cornille" and "Safronova" data sets compiled by Kato et al. (1997) results in notable discrepancies that undermine confidence in spectral modeling. Moreover, with the exception of the extensive study by Jacobs et al. (1989), there has hardly been any attention in ions with $N > 6$. In the present work, *A*-values for the allowed and forbidden valence–valence transitions within the $n = 2$ complex have also been treated because the post-Auger radiative signature, rich in UV and optical emission lines, has been shown to have astrophysical potential (Shapiro & Bahcall 1981).

The details of the computational approach and of the approximations considered are given in Sects. 2–3, as well as

those of previously available data sets that are brought in for comparison purposes. Results, namely energy levels, *A*-values and Auger rates, are discussed in Sects. 4–6 ending with a summary and conclusions in Sect. 7.

## 2. Numerical methods

The present computational approach is based on standard atomic physics codes, namely AUTOSTRUCTURE, HFR, and BPRM, rather than on in-house developments. They have been widely used in the past thirty years to study valence-electron processes and more recently to the inner shells. These packages allow the inclusion of electron-correlation effects, core relaxation, relativistic corrections and semiempirical fine tuning. Radiative and collisional data are computed for $N$- or $(N+1)$-electron systems in a relativistic Breit–Pauli framework

$$H_{\rm bp} = H_{\rm nr} + H_{\rm 1b} + H_{\rm 2b} \quad (1)$$

where $H_{\rm nr}$ is the usual non-relativistic Hamiltonian. The one-body relativistic operators

$$H_{\rm 1b} = \sum_{n=1}^{N} f_n({\rm mass}) + f_n({\rm d}) + f_n({\rm so}) \quad (2)$$

represent the spin–orbit interaction, $f_n$(so), and the non-fine structure mass-variation, $f_n$(mass), and one-body Darwin, $f_n$(d), corrections. The two-body corrections

$$H_{\rm 2b} = \sum_{n>m} g_{nm}({\rm so}) + g_{nm}({\rm ss}) + g_{nm}({\rm css}) + g_{nm}({\rm d}) + g_{nm}({\rm oo}), \quad (3)$$

usually referred to as the Breit interaction, include, on the one hand, the fine structure terms $g_{nm}$(so) (spin–other-orbit and mutual spin–orbit) and $g_{nm}$(ss) (spin–spin), and on the other, the non-fine structure terms: $g_{nm}$(css) (spin–spin contact), $g_{nm}$(d) (two-body Darwin), and $g_{nm}$(oo) (orbit–orbit).

### 2.1. AUTOSTRUCTURE

AUTOSTRUCTURE (Badnell 1986, 1997), based on the popular atomic structure code SUPERSTRUCTURE (Eissner et al. 1974), computes relativistic fine structure level energies, *A*-values and Auger rates. Configuration-interaction (CI) wavefunctions are constructed from single-electron orbitals generated in a statistical Thomas–Fermi–Dirac potential (Eissner & Nussbaumer 1969). Continuum wavefunctions are obtained in a distorted-wave approximation. The Breit–Pauli implementation includes to order $\alpha^2 Z^4$ the one- and two-body operators (fine structure and non-fine structure) of Eqs. (2–3) where $\alpha$ is the fine structure constant and $Z$ the atomic number. Fine tuning takes the form of term energy corrections (TEC) where an improved relativistic wavefuntion, $\psi_i^{\rm r}$, is obtained in terms of the non-relativistic functions

$$\psi_i^{\rm r} = \psi_i^{\rm nr} + \sum_{j\neq i} \psi_j^{\rm nr} \times \frac{\langle \psi_j^{\rm nr} | H_{\rm 1b} + H_{\rm 2b} | \psi_i^{\rm nr} \rangle}{E_i^{\rm nr} - E_j^{\rm nr}} \,, \quad (4)$$

with the $LS$ term energy differences $(E_i^{\rm nr} - E_j^{\rm nr})$ adjusted to fit the centers of gravity of the experimental multiplets. This procedure thus relies on the availability of spectroscopic data.

### 2.2. HFR

In the HFR code by Cowan (1981), an orbital basis is obtained for each electronic configuration by solving the Hartree–Fock equations for the spherically averaged atom. The equations result from the application of the variational principle to the configuration average energy and include relativistic corrections, namely the Blume–Watson spin–orbit, mass-variation and one-body Darwin terms. The Blume–Watson spin–orbit term comprises the part of the Breit interaction that can be reduced to a one-body operator. The radial integrals can be adjusted to reproduce the experimental energy levels by least-squares fitting procedures. The eigenvalues and eigenstates thus obtained (ab initio or semiempirically) are used to compute the wavelength and *A*-value for each possible transition. Autoionization rates are calculated in a perturbation theory scheme where the radial functions of the initial and final states are optimized separately, and CI is accounted for only in the autoionizing state.

### 2.3. BPRM

The Breit–Pauli *R*-matix suite (BPRM) is based on the close-coupling approximation of Burke & Seaton (1971) whereby the wavefunctions for states of an $N$-electron target and a colliding electron with total angular momentum and parity $J\pi$ are expanded in terms of the target eigenfunctions

$$\Psi^{J\pi} = \mathcal{A} \sum_i \chi_i \frac{F_i(r)}{r} + \sum_j c_j \Phi_j \,. \quad (5)$$

The functions $\chi_i$ are vector coupled products of the target eigenfunctions and the angular part of the incident-electron functions, $F_i(r)$ are the radial part of the latter and $\mathcal{A}$ is an antisymmetrization operator. The functions $\Phi_j$ are bound-type functions of the total system constructed with target orbitals; they are introduced to compensate for orthogonality conditions imposed on the $F_i(r)$ and to improve short-range correlations. The Kohn variational principle gives rise to a set of coupled integro-differential equations that are solved by *R*-matrix techniques (Burke et al. 1971; Berrington et al. 1974, 1978, 1987) within a box of radius, say, $r \leq a$. In the asymptotic region ($r > a$), resonance positions and widths are obtained from fits of the eigenphase sums with the STGQB module developed by Quigley & Berrington (1996) and Quigley et al. (1998). Normalized partial widths are defined from projections onto the open channels. Breit–Pauli relativistic corrections have been introduced in the *R*-matrix suite by Scott & Burke (1980) and Scott & Taylor (1982), but the two-body terms (see Eq. (3)) have not as yet been incorporated.

## 3. Approximations and external data sets

Following the scheme employed in Paper I, we compute data sets in several approximations and compare with external data sets to bring out the relevant physical effects and the degree of precision that can be attained.

**AST1**: Data are computed with AUTOSTRUCTURE, the ion being modeled with an orthogonal orbital basis obtained by minimizing the sum of all the $LS$ terms. It includes configurations

only within the $n = 2$ complex and excludes the Breit interaction (i.e. the two-body terms in Eq. (3)).

**AST2**: The same as AST1 but includes the Breit interaction.

**AST3**: As AST2 but the ion representation now includes single and double excitations within the $n \leq 3$ complexes, and level energies are fine-tuned with TEC with reference to the measured levels in data set EXP1. In the case of unobserved levels, the TEC have been estimated from the reported values. This is our best approximation.

**AST3′**: The same as AST3 but without TEC.

**HFR3**: A computation with HFR where the ion is represented with a set of non-orthogonal orbitals for each configuration obtained by optimizing its average energy. It includes single and double excitations within the $n \leq 3$ complexes, and the radial integrals are fitted to reproduce the experimental energies. In the case of unobserved levels, the theoretical levels have not been adjusted. HFR3 is expected to give results comparable to AST3.

**HFR3′**: The same as HFR3 but without semiempirical corrections.

**BPR1**: A BPRM computation where the ion targets are modeled with configurations within the $n = 2$ complex. Since the code excludes the Breit interaction, this approximation is comparable to AST1.

**EXP1**: Contains the experimental level energies for Fe XVIII–Fe XXV listed in the critical compilation of Shirai et al. (2000), except for the $1s2s^2 2p^4\ ^2L_j$ levels in Fe XX and the $1s2s^2 2p^6\ ^2S_{1/2}$ level in Fe XVIII where energies are derived from the laboratory wavelengths in data set EXP2. Present calculations suggest that these level energies, which have been obtained from flare spectra (Seely et al. 1986; Feldman et al. 1980), are poor. In this respect, Beiersdorfer et al. (1993) have previously questioned the solar identifications of the F1 and F2 lines of the F-like species.

**EXP2**: Includes 78 wavelengths reported for Fe XVIII–Fe XXV in the tokamak measurements by Beiersdorfer et al. (1993) and in experiments with an electron beam ion trap (Decaux et al. 1997). In the case of duplicate measurements, we assume the most recent as the most accurate as error bars were not reported by Decaux et al. The transition labeled O2 has been excluded due to a questionable assignment.

**SAF**: This external data set includes energy levels listed by Safronova & Shlyaptseva (1996, 1999) for Fe ions with electron occupancy $3 \leq N \leq 9$; wavelengths, $A$-values and total Auger rates for $3 \leq N \leq 6$ compiled in the "Safronova" data set by Kato et al. (1997); and partial Auger rates for $N = 5$ reported by Safronova et al. (1998). They have been computed with the MZ code (Safronova & Urnov 1980) which uses a hydrogenic orbital basis, includes electron correlation effects, the Breit interaction and QED contributions estimated in a hydrogenic approximation through screening constants.

**COR**: Corresponds to the "Cornille" data set compiled by Kato et al. (1997) which tabulates wavelengths, $A$-values and total Auger rates for ions with $3 \leq N \leq 6$, and the partial Auger rates for $N = 5$ reported by Safronova et al. (1998). The data have been calculated with the program AUTOLSJ of Dubau & Loulergue (1981), an independent but similar implementation of AUTOSTRUCTURE.

**MCDF**: Wavelengths, $A$-values and Auger (total and partial) rates computed in a multi-configuration Dirac–Fock method by Chen (1986), Chen & Crasemann (1987, 1988) and Chen et al. (1997) for ions with $3 \leq N \leq 6$. The Breit interaction and QED corrections are taken into account in the energy calculations. CI is only assumed within the $n = 2$ complex.

**HFR4**: Wavelengths, $A$-values, satellite intensity $Q_\mathrm{d}$ factors, and radiative branching ratios, $B_\mathrm{r}$, calculated for Fe XVIII–Fe XXIV by Jacobs et al. (1989) with HFR. This external data set includes only the dominant transitions listed in Table III and IV of this paper.

Levels are to be addressed with the notation $(N; i)$, $N$ being the electron occupancy of the ion and $i$ the level index, and $k \to i$ downward transitions as $(N; k, i)$ where in the case of an Auger process the $i$th level belongs to the $(N-1)$-electron ion. The radiative and Auger widths of the $k$ level are given by

$$A_\mathrm{r}(k) = \sum_i A_\mathrm{r}(k,i) \quad \text{and} \quad A_\mathrm{a}(k) = \sum_i A_\mathrm{a}(k,i) \tag{6}$$

where $A_\mathrm{r}(k,i)$ and $A_\mathrm{a}(k,i)$ are respectively the radiative and Auger rates. The $\mathrm{K}_\alpha$ fluorescence yield of a level is then given by

$$\omega_\alpha(k) = \frac{A_\mathrm{r}(k)}{A_\mathrm{r}(k) + A_\mathrm{a}(k)}. \tag{7}$$

For a transition, the radiative branching ratio is expressed as

$$B_\mathrm{r}(k,i) = \frac{A_\mathrm{r}(k,i)}{A_\mathrm{r}(k) + A_\mathrm{a}(k)} \tag{8}$$

and its the satellite intensity factor as

$$Q_\mathrm{d}(k,i) = g(k) B_\mathrm{r}(k,i) A_\mathrm{a}(k)\ . \tag{9}$$

where $g(k)$ is the statistical weight of the upper level.

Since most comparisons involve data sets of relatively large volumes, we introduce simple statistical indicators. For energy and wavelength data sets, $X$ and $Y$ say, average energy and wavelength differences are defined as

$$\overline{\Delta E}(Y,X) = \frac{1}{M} \sum_{m=1}^{M} E(Y_m) - E(X_m) \tag{10}$$

and

$$\overline{\Delta \lambda}(Y,X) = \frac{1}{M'} \sum_{m=1}^{M'} \lambda(Y_m) - \lambda(X_m) \tag{11}$$

while for rates, $A(X)$ and $A(Y)$, comparisons are more conveniently carried out in terms of an average ratio

$$\overline{R}(Y,X) = \frac{1}{M''} \sum_{m=1}^{M''} \frac{A(Y_m)}{A(X_m)}. \tag{12}$$

Similarly, average ratios $\overline{R}_{B_\mathrm{r}}(Y,X)$ and $\overline{R}_{Q_\mathrm{d}}(Y,X)$ can be defined for comparisons of branching ratios and satellite intensity factors.

## 4. Level energies and wavelengths

In the computation of the decay properties of K-vacancy states, it is essential to ensure adequate representations of both the upper resonances and the lower bound valence states, and therefore level energy comparisons must pay attention to both groups. In Table 1 we present the energies for the 217 fine structure levels that take part in the decay of the $n = 2$ K-vacancy states in Fe XVIII–Fe XXV. Following conclusions in Paper I, they have been calculated in what we regard our best approximation: AST3. They are also compared with 131 spectroscopic values from the data set EXP1 resulting in a mean energy difference of $\overline{\Delta E}$(EXP1, AST3) = $-0.1 \pm 0.5$ eV. The larger discrepancies (less than 1.8 eV) appear for the (5;20–23) and (6;22–24) levels. They belong to spectroscopic terms that are strongly mixed within the configurations $1s2s^22p^2$ in Fe XXII and $1s2s^22p^3$ in Fe XXI; more precisely, the $^2$D and $^2$P in the B-like ion and the $^3$D$^o$, $^1$D$^o$ and $^3$P$^o$ in the C-like are so mixed that the TEC procedure has been helpful in getting the correct term order. Moreover, the TEC have improved appreciably the theoretical level energies since $\overline{\Delta E}$(EXP1, AST3′) = $-6.6 \pm 6.9$ eV. The ab initio eigenvalues obtained with HFR agree better with the experiment, i.e. $\overline{\Delta E}$(EXP1, HFR3′) = $-1.4 \pm 2.7$ eV, as it allows for core relaxation effects by using non-orthogonal orbitals for each configuration. By contrast, the single-electron orbitals in AUTOSTRUCTURE have been optimized by minimizing all the term energies included in the atomic model.

Level energies in AST3 for ions with electron occupancies of $3 \le N \le 9$ have also been compared with a complete HFR3 set and with 189 values in SAF (21 levels in Fe XXI and 1 in Fe XX have not been quoted in SAF) leading to mean energy differences of $\overline{\Delta E}$(HFR3, AST3) = $0.6 \pm 2.2$ eV and $\overline{\Delta E}$(SAF, AST3) = $0.0 \pm 3.0$ eV. The larger differences with HFR3 (up to 3.7 eV) are encountered in levels within the $1s2s^22p^3$ configuration of Fe XXI, i.e. (6; 22–30). This is a particularly difficult spectral interval with strongly mixed components, questionable spectroscopic identifications and sensitive fine structure splittings. Furthermore, levels belonging to configurations which have not been corrected in HFR3 due to the absence of reported measurements, mainly (6;31–50), (7;24–31) and (8;15–16), are systematically 5–7 eV higher than AST3. In the comparison with SAF, the (5;36), (5;39) and (5;42) levels have been excluded due to unusually gross discrepancies (up to 41 eV) which are probably due to misquoted data in SAF. Although the accuracy of the level energies in AST3 is strongly linked to that of EXP1 due to the TEC, it has been possible to present a complete set of levels with a statistical accuracy estimated at ±3 eV.

In Table 2 wavelengths for 937 transitions are listed. They include transitions arising from the K-vacancy resonances as well as those among the $n = 2$ valence levels. They have been determined from the experimental level energies when available otherwise from those in approximation AST3, and for convenience the data set will be referred to hereafter with this label. A comparison with the 78 measured values in data set EXP2 results in a mean difference of $\overline{\Delta\lambda}$(EXP2, AST3) = $0.0 \pm 1.0$ mÅ where the experimental wavelengths $\lambda(7;22,1)$ = 1.90477 Å (labeled N5), $\lambda(7;20,5)$ = 1.91359 Å (N14) and $\lambda(7;16,3)$ = 1.91312 Å (N15) are believed to be in error well outside the quoted experimental accuracy of a few tenths of a mÅ. When wavelengths in AST3 are compared with the other theoretical data sets, results are also encouraging and suggest a statistical accuracy rating of ±2 mÅ. Values in HFR3 for 888 transitions involving K resonances in species with $3 \le N \le 9$ are on average somewhat shorter since $\overline{\Delta\lambda}$(HFR3, AST3) = $-0.4 \pm 0.8$ mÅ, specially for transitions involving unadjusted levels, e.g. (7;24–31). In the case of the 219 transitions listed in HFR4, wavelengths are even shorter: $\overline{\Delta\lambda}$(HFR4, AST3) = $-2.2 \pm 0.9$ mÅ. This indicates that Jacobs et al. (1989) computed wavelengths with ab initio level energies. COR, SAF and MCDF respectively give values for 73, 101 and 497 transitions in ions with $4 \le N \le 6$. The following mean wavelength differences with AST3 are obtained: $\overline{\Delta\lambda}$(COR, AST3) = $-3.5 \pm 1.0$ mÅ, $\overline{\Delta\lambda}$(SAF, AST3) = $0.2 \pm 1.2$ mÅ and $\overline{\Delta\lambda}$(MCDF, AST3) = $0.2 \pm 2.0$ mÅ. With reference to COR, the present findings are consistent with those in Paper I regarding their wavelengths being systematically shorter by ∼3 mÅ. In MCDF discrepancies as large as 10 mÅ are found for the (5;*k*,8–9) and (6;44,*i*) transitions.

## 5. Radiative rates

The radiative rates and total radiative widths computed with approximation AST3 are listed in Tables 1–2. In order to estimate their accuracy, we have considered several effects that have been found relevant in Paper I: CI, Breit interaction, fine tuning and their variations along the isonuclear sequence. It is found that CI from configurations with $n = 3$ orbitals is of little importance and can be practically neglected. The contributions of the Breit interaction are brought out by comparing *A*-values computed with approximations AST1 and AST2 for species with $3 \le N \le 8$ as shown in Fig. 1. The general trend is that differences become more conspicuous for the weaker transitions, from ∼10% for those with $\log A_r > 14$ to several orders of magnitude for the smaller rates. This trend is broken for 3 notorious transitions with $\log A_r > 13$ in the C-like system: (6;29,3–4) and (6;26,4). The upper energy levels of these transitions belong to the strongly mixed $^1$D$^o$ and $^3$P$^o$ terms of $1s2s^22p^3$ discussed in Sect. 4. In this instance, the spin–spin coupling causes drastic changes. If they are put aside, the average ratios for transitions with $\log A_r > 13$ listed in Table 3 for the AST1/AST2 data sets indicate that this effect is of the order of ∼15% and does not decrease with *N*. Changes originating from fine tuning (TEC) – see $\overline{R}$(AST2, AST3) in Table 3 – display a similar behavior and are not larger (less than 17%) if a few sensitive transitions are excluded, namely (4;20,4), (6;26,3–4), (6;28,2) and (6;29,4).

The key comparison is between AST3 and HFR3 for many reasons: they are two independent numerical methods which have been used to generate complete sets of *A*-values; their fine tuning capabilities follow different approaches, AUTOSTRUCTURE employs TEC (see Sect. 2.1) whereas HFR relies on the treatment of radial integrals as fitting parameters; and their respective weaknesses have been well established in Paper I, the former by adopting an orthogonal orbital basis which excludes core relaxation effects and the latter with a reduced

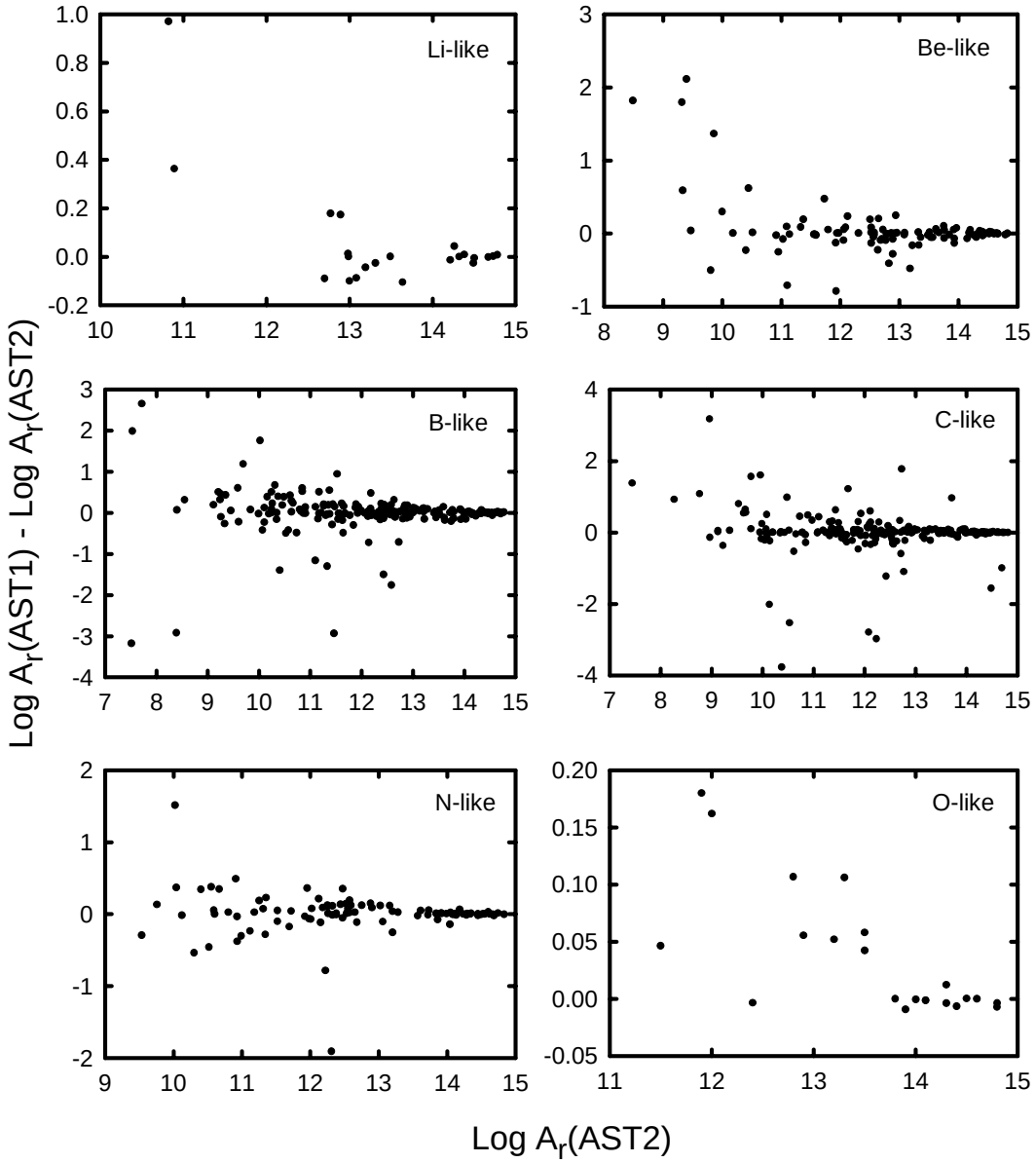


**Fig. 1.** Comparison of *A*-values ($s^{-1}$) computed in approximations AST1 and AST2 for Fe ions with $3 \leq N \leq 8$. Differences are due to the contribution of the Breit interaction.

implementation of the Breit interaction. It is shown in Fig. 2 and Table 3 that for $\log A_r > 13$ AST3 and HFR3 contain *A*-values that agree to within 20%, an acceptable level of accuracy mainly limited by code options. This result certainly establishes a milestone for evaluating previous work.

Although the HFR4 rates are on average slightly higher by ∼3–6% as shown in Table 3 and Fig. 2, the agreement with AST3 is also within 20% (see Fig. 2). Rates in COR and SAF agree with those in AST3 to ∼20% (see Fig. 3 and Table 3) if a handful of transitions with discrepancies larger than a factor of 2 are excluded: (6;23,4), (6;26,4) and (6;29,4) in COR and those listed in Table 4 in SAF. On the other hand, it may be seen in Fig. 3 that the number of transitions in MCDF displaying large discrepancies with AST3 is noticeably larger. These transitions are listed in Table 5 and were excluded from the statistical indicators of Table 3. A contrasting and worrying aspect is that while the mean ratios for $N \leq 5$ are within a comparable accuracy interval (∼17%), that for the C-like ion indicates *A*-values that are on average 20% higher with a scatter of the order of 30%. This finding seems to point out at numerical problems in the MCDF radiative data for Fe XXI.

## 6. Auger decay data

Auger widths computed in approximation AST3 for the K-vacancy levels of the $n = 2$ complex in Fe XVIII–Fe XXIV are presented in Table 1. It can be seen that while levels in ions with $N > 4$ have Auger widths of $\log A_a(i) > 14$, with the sole exception of the sextet (5; 19), levels in the Li- and Be-like systems have widths as low as $10^9$ $s^{-1}$ making them more susceptible to the approximation level. This assertion is supported by the mean ratios $\overline{R}$(BPR1, AST1) for $3 \leq N \leq 9$ given in Table 6 where standard deviations of 14% and 11% for Fe XXIV and Fe XXIII, respectively, decrease to ∼5% in species

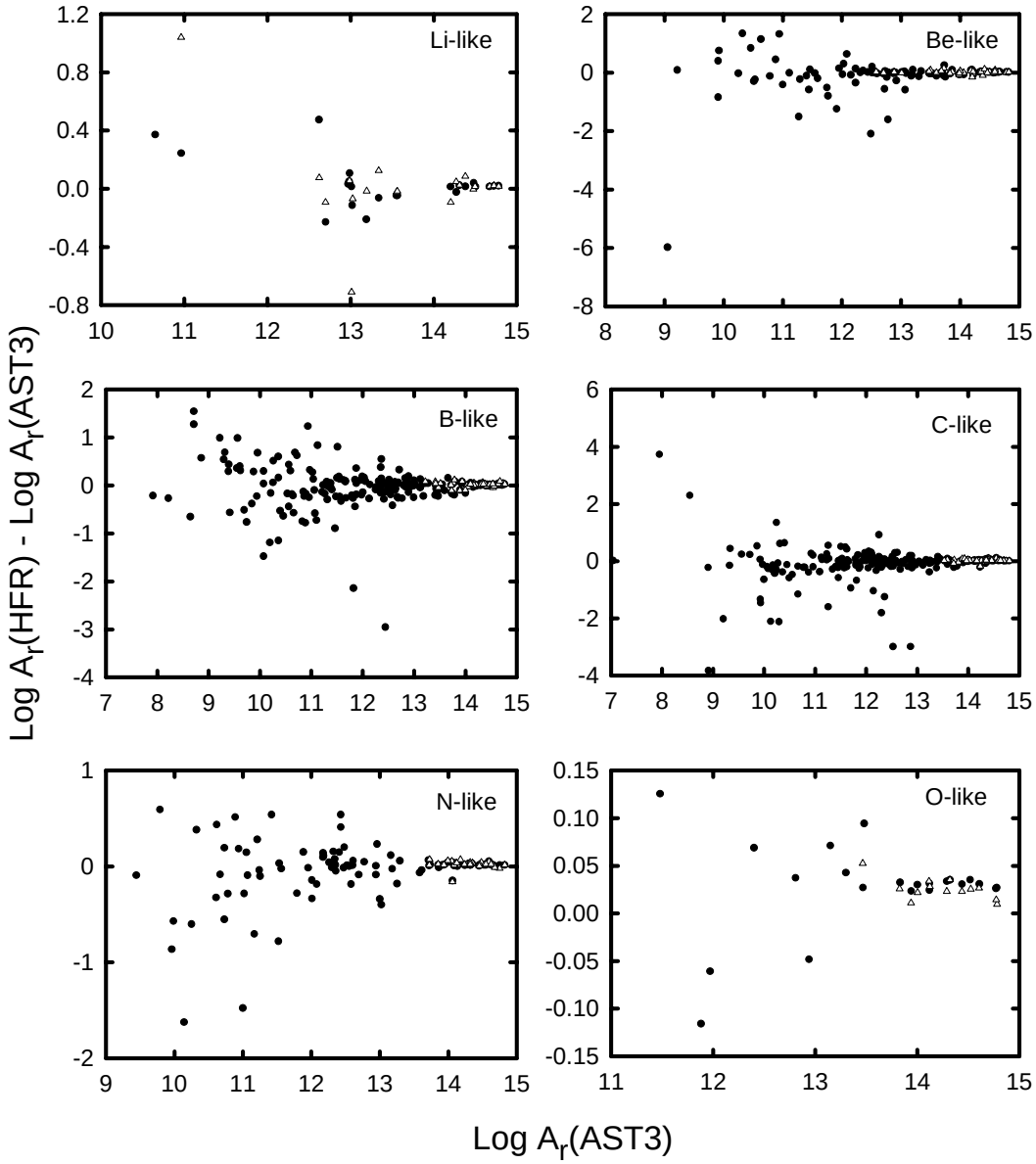


**Fig. 2.** Comparison of $A$-values ($s^{-1}$) computed in approximations HFR3 (filled circles) and HFR4 (triangles) with AST3 for Fe ions with $3 \leq N \leq 8$. An agreement of ~20% is found for transitions with $\log A_r > 13$.

with $N > 4$. It is found that extra-complex configuration interaction and TEC have small effects on the total Auger rates.

An important finding realized in Paper I in connection with the Auger decay of the Li-like Fe species has been the conspicuous role of the Breit interaction; that is, the prominence of the spin–spin coupling not only between bound levels but also involving the final continuum states, a fact that was not always given adequate attention in previous work. We are therefore concerned with its $N$ behaviour which can be discerned by comparing approximations AST1 and AST2 (see Table 6). It is found that the Breit interaction on average decreases Auger rates by as much as 10% for ions with low $N$ but is reduced to 4% for $N = 9$. The larger differences (30% to a factor of 2) are found for the (3;5–7), (3;10) and (3;13–14) quartet levels in Fe XXIV and the (4;14–16) and (4;28) quintet levels in Fe XXIII that autoionize via intersystem or magnetically coupled channels. By examining mean ratios for approximations HFR3 and AST3 in Table 6, it can be inferred that discrepancies are mostly due to the neglect of core relaxation in AUTOSTRUCTURE and to the treatment of relativistic corrections in HFR as concluded in Paper I. The HFR package can hardly cope with strong Breit coupling, as indicated by the poor agreement for ions with $N \leq 4$, but for the less ionized system the statistical agreement is better than 10%.

The good statistical accord (better than 10%) obtained with three different numerical methods for the Auger rates in ions with $N > 4$ provides a second milestone for evaluating external data sets. A comparison of total rates in COR, SAF and MCDF with those in our best approximation (AST3) are shown in Fig. 4 and Table 6. The discrepancies with COR, as discussed in Paper I, are well understood in terms of their neglect of the Breit interaction and thus decrease rapidly with $N$.

**Table 3.** Comparison of *A*-value data sets for Fe XVIII–Fe XXIV in terms of mean ratios.

| Data sets[a] | Fe XXIV | Fe XXIII | Fe XXII | Fe XXI | Fe XX | Fe XIX | Fe XVIII |
|---|---|---|---|---|---|---|---|
| $\overline{R}$(AST1, AST2) | 0.95 ± 0.09 | 0.98 ± 0.15 | 1.01 ± 0.15 | 1.00 ± 0.12[b] | 1.00 ± 0.12 | 1.04 ± 0.08 | 1.00 |
| $\overline{R}$(AST2, AST3) | 1.01 ± 0.08 | 1.00 ± 0.17[c] | 1.00 ± 0.07 | 0.99 ± 0.11[d] | 1.00 ± 0.08 | 1.00 ± 0.02 | 1.00 |
| $\overline{R}$(HFR3, AST3) | 0.96 ± 0.13 | 1.00 ± 0.16 | 1.00 ± 0.16 | 1.00 ± 0.17 | 1.01 ± 0.16 | 1.09 ± 0.07 | 1.05 |
| $\overline{R}$(HFR4, AST3) | 1.03 ± 0.13[e] | 1.06 ± 0.13 | 1.05 ± 0.10 | 1.05 ± 0.09 | 1.05 ± 0.08 | 1.06 ± 0.03 | 1.06 |
| $\overline{R}$(COR, AST3) | 0.96 ± 0.09 | 1.01 ± 0.17 | 0.95 ± 0.16 | 0.95 ± 0.23[f] | | | |
| $\overline{R}$(SAF, AST3) | 1.02 ± 0.04 | 1.00 ± 0.23[g] | 0.96 ± 0.16[h] | 1.00 ± 0.18[i] | | | |
| $\overline{R}$(MCDF, AST3) | 0.95 ± 0.05 | 1.03 ± 0.17[j] | 0.96 ± 0.14[k] | 1.18 ± 0.28[l] | | | |

[a] Comparison includes only transitions with $\log A_r > 13$.
[b] Excludes transitions (6;29,3–4) and (6;26,4).
[c] Excludes transition (4;20,4).
[d] Excludes transitions (6;26,3–4), (6;28,2) and (6;29,4).
[e] Excludes transition (3;19,2).
[f] Excludes transitions (6;23,4), (6;26,4) and (6;29,4).
[g] Excludes transitions (4;25–24,3), (4;20,4) and (4;24,4) in Table 4.
[h] Excludes transitions (5;43,13), (5;46,15) and (5;49,15) in Table 4.
[i] Excludes transitions (6;26,3–4) and (6;29,4) in Table 4.
[j] Excludes transitions (4;20,4) and (6;38,9) in Table 5.
[k] Excludes transitions (5;*k*,*i*) in Table 5.
[l] Excludes transitions (6;*k*,*i*) in Table 5.

**Table 4.** Radiative transition rates ($s^{-1}$) in SAF that show large discrepancies with AST3. Note: $a \pm b \equiv a \times 10^{\pm b}$.

| *N* | *k* | *i* | SAF | AST3 | HFR3 | HFR4 | COR | MCDF |
|---|---|---|---|---|---|---|---|---|
| 4 | 20 | 4 | 8.17 + 12 | 1.59 + 13 | 1.98 + 13 | | 2.61 + 13 | 2.84 + 13 |
| 4 | 24 | 3 | 8.85 + 13 | 3.99 + 13 | 3.11 + 13 | 4.00 + 13 | 4.23 + 13 | 3.44 + 13 |
| 4 | 24 | 4 | 3.67 + 13 | 9.55 + 13 | 8.37 + 13 | 8.20 + 13 | 7.95 + 13 | 1.04 + 14 |
| 4 | 25 | 3 | 2.13 + 14 | 1.00 + 14 | 1.00 + 14 | 1.13 + 14 | | 8.27 + 13 |
| 5 | 43 | 13 | 2.40 + 12 | 1.66 + 13 | 1.82 + 13 | 2.00 + 13 | | 1.67 + 13 |
| 5 | 46 | 15 | 1.40 + 14 | 3.93 + 13 | 3.08 + 13 | | | 4.19 + 13 |
| 5 | 49 | 15 | 2.67 + 13 | 1.42 + 14 | 1.32 + 14 | | | 1.31 + 14 |
| 6 | 26 | 3 | 4.70 + 12 | 3.10 + 14 | 3.13 + 14 | 3.39 + 14 | | 6.26 + 12 |
| 6 | 26 | 4 | 4.86 + 14 | 1.70 + 14 | 1.05 + 14 | 1.14 + 14 | 4.85 + 14 | 6.05 + 14 |
| 6 | 29 | 4 | 6.89 + 13 | 3.53 + 14 | 4.63 + 14 | 4.46 + 14 | 5.82 + 13 | 6.58 + 13 |

In contrast, differences with SAF for $3 \le N \le 6$ are sustainedly higher by as much as 30% and increase with *N*, a trend difficult to explain. The situation with respect to MCDF is also curious as the statistical agreement with AST3 is good (better that 10%) for $N \le 5$ but for the C-like species it singularly deteriorates. Comparison with HFR4 can only be carried out in terms of satellite intensity factors and radiative branching ratios. As shown in Table 7, sizable discrepancies are not only found for $N \le 4$ as expected of the **HFR** method, but more surprizingly in the C-like and N-like ions.

Level-to-level (partial) Auger rates have also been calculated with approximation AST3 and are listed in Table 8. We have found in this work that the **BPRM** and **HFR** codes are not currently usable for the computation of partial Auger rates. In this respect, the **STGQB** module in the **BPRM** package lists asymptotic channel weights from which partial widths can be obtained. However, this procedures is deficient in the case of low-*n* resonances which have most of their wavefunctions within the *R*-matrix inner region, and thus the asymptotic weights are not really representative of channel strengths; we have found hardly any accord between the partial rates in BPR1 and AST1 in spite of the matching of the total widths. In **HFR**, the only information available about the target states are the *LS* parent terms of the continuum states. Consequently, partial Auger rates of autoionizing levels decaying to *LS* terms of the $(N-1)$-electron ion can only be determined. If partial rates with $\log A_a < 13$ are put aside, the contribution of the Breit interaction is on average less than 20% but does not decrease with *N*. TEC also cause the more sizable differences in Fe XXI (10%) and Fe XX (14%) with the exception of the transitions (6;29,*i*) and (7;18,7–8) where they can reach a factor of 2. As can be seen in Fig. 5, the conclusions derived from the comparisons

**Table 5.** Radiative transition rates ($s^{-1}$) in MCDF that show large discrepancies with AST3. Note: $a \pm b \equiv a \times 10^{\pm b}$.

| $N$ | $k$ | $i$ | MCDF | AST3 | HFR3 | HFR4 | COR | SAF |
|---|---|---|---|---|---|---|---|---|
| 4 | 20 | 4 | 2.84 + 13 | 1.59 + 13 | 1.98 + 13 | | 2.61 + 13 | 8.17 + 12 |
| 4 | 38 | 9 | 7.14 + 12 | 1.55 + 13 | 1.30 + 13 | | | |
| 5 | 33 | 8 | 7.87 + 12 | 5.81 + 13 | 6.36 + 13 | 6.70 + 13 | | |
| 5 | 36 | 6 | 3.75 + 11 | 2.15 + 14 | 2.37 + 14 | 2.49 + 14 | | |
| 5 | 36 | 7 | 1.99 + 14 | 7.77 + 13 | 6.25 + 13 | 6.10 + 13 | | |
| 5 | 36 | 9 | 1.19 + 11 | 1.50 + 13 | 9.05 + 12 | | | |
| 5 | 39 | 7 | 8.96 + 13 | 2.19 + 14 | 2.39 + 14 | 2.41 + 14 | | |
| 5 | 39 | 10 | 5.26 + 11 | 1.48 + 13 | 1.62 + 13 | | | |
| 5 | 41 | 7 | 8.18 + 12 | 1.48 + 13 | 1.65 + 13 | | | |
| 5 | 41 | 9 | 1.23 + 10 | 1.03 + 13 | 1.09 + 13 | | | |
| 5 | 42 | 9 | 1.84 + 09 | 8.54 + 13 | 1.02 + 14 | 1.05 + 14 | | |
| 6 | 26 | 3 | 6.26 + 12 | 3.10 + 14 | 3.13 + 14 | 3.39 + 14 | | 4.70 + 12 |
| 6 | 26 | 4 | 6.05 + 14 | 1.70 + 14 | 1.05 + 14 | 1.14 + 14 | 4.85 + 14 | 4.86 + 14 |
| 6 | 28 | 2 | 8.18 + 10 | 1.73 + 13 | 7.25 + 12 | | | |
| 6 | 29 | 4 | 6.58 + 13 | 3.53 + 14 | 4.63 + 14 | 4.46 + 14 | 5.82 + 13 | 6.89 + 13 |
| 6 | 34 | 7 | 5.63 + 12 | 4.23 + 13 | 4.31 + 13 | | | |
| 6 | 34 | 8 | 2.79 + 10 | 4.10 + 14 | 4.45 + 14 | 4.41 + 14 | | |
| 6 | 34 | 9 | 4.94 + 14 | 2.18 + 14 | 1.82 + 14 | 1.98 + 14 | | |
| 6 | 37 | 8 | 5.77 + 14 | 5.19 + 13 | 3.11 + 13 | 4.30 + 13 | | |
| 6 | 37 | 9 | 1.03 + 14 | 2.21 + 14 | 2.66 + 14 | 2.43 + 14 | | |
| 6 | 37 | 11 | 1.13 + 13 | 1.65 + 14 | 1.74 + 14 | 1.75 + 14 | | |
| 6 | 38 | 11 | 6.58 + 13 | 2.59 + 13 | 3.69 + 13 | | | |
| 6 | 38 | 13 | 4.24 + 12 | 1.10 + 13 | 1.06 + 13 | | | |
| 6 | 40 | 10 | 2.21 + 12 | 1.28 + 13 | 9.07 + 12 | | | |
| 6 | 42 | 11 | 3.72 + 13 | 8.47 + 13 | 9.11 + 13 | 1.04 + 14 | | |
| 6 | 43 | 13 | 7.83 + 12 | 2.40 + 13 | 2.31 + 13 | | | |
| 6 | 44 | 12 | 1.50 + 12 | 9.76 + 13 | 1.07 + 14 | 1.09 + 14 | | |
| 6 | 44 | 13 | 3.91 + 12 | 2.12 + 14 | 2.17 + 14 | 2.23 + 14 | | |
| 6 | 44 | 14 | 5.84 + 14 | 4.41 + 13 | 4.86 + 13 | | | |
| 6 | 45 | 14 | 8.58 + 13 | 4.92 + 14 | 5.09 + 14 | 5.04 + 14 | | |
| 6 | 45 | 15 | 2.00 + 12 | 2.86 + 14 | 2.96 + 14 | 2.97 + 14 | | |

**Table 6.** Comparison of Auger rate data sets for Fe XVIII–Fe XXIV in terms of mean ratios.

| Data sets | Fe XXIV | Fe XXIII | Fe XXII | Fe XXI | Fe XX | Fe XIX | Fe XVIII |
|---|---|---|---|---|---|---|---|
| $\overline{R}$(AST1, AST2) | 1.10 ± 0.24 | 1.11 ± 0.29 | 1.05 ± 0.09 | 1.04 ± 0.03 | 1.04 ± 0.02 | 1.04 ± 0.02 | 1.04 |
| $\overline{R}$(BPR1, AST1) | 0.99 ± 0.14 | 0.98 ± 0.11 | 0.98 ± 0.04 | 1.00 ± 0.02 | 1.01 ± 0.02 | 1.03 ± 0.01 | 1.06 |
| $\overline{R}$(HFR3, AST3) | 1.68 ± 2.18 | 1.06 ± 0.25 | 1.00 ± 0.08 | 1.00 ± 0.03 | 1.01 ± 0.02 | 1.03 ± 0.02 | 1.03 |
| $\overline{R}$(COR, AST3) | 1.06 ± 0.20 | 1.04 ± 0.27 | 0.99 ± 0.10 | 0.95 ± 0.06 | | | |
| $\overline{R}$(SAF, AST3) | 1.08 ± 0.15 | 1.16 ± 0.23 | 1.21 ± 0.27 | 1.28 ± 0.04 | | | |
| $\overline{R}$(MCDF, AST3) | 0.96 ± 0.33 | 1.02 ± 0.08 | 1.04 ± 0.04 | 1.20 ± 0.19 | | | |

of the total rates of AST3 with COR, SAF and MCDF are but asserted when their partial rates for ions with $3 \leq N \leq 6$ are analyzed.

## 7. Summary and conclusions

We have successfully extended the multi-code approach of Paper I to generate a complete set of radiative and Auger decay data for the $n = 2$ K-vacancy states in ionic species of the first row of the Fe isonuclear sequence, and to provide reliable estimates of their accuracy. The data set also includes radiative rates for both the allowed and forbidden transitions among the $n = 2$ valence levels that become the primary receptacles of the inner-shell decay tree. Their multi-wavelength spectral signature can lead to astrophysical diagnostics (Shapiro & Bahcall 1981).

The Breit interaction must be taken into account throughout in order to maintain accuracy, in particular for transitions with small rates and for those involving levels subject to strong relativistic couplings which in most cases are difficult to predict in advance. Although our ab initio calculations provide sufficiently accurate level energies especially in the case of HFR,

**Table 7.** Comparison of satellite intensity $Q_d$ factors and radiative branching ratios, $B_r$, for Fe XVIII–Fe XXIV in terms of mean ratios.

| Data sets | Fe XXIV | Fe XXIII | Fe XXII | Fe XXI | Fe XX | Fe XIX | Fe XVIII |
|---|---|---|---|---|---|---|---|
| $\overline{R}_{Q_d}$(HFR4, AST3) | 2.29 ± 2.75 | 1.02 ± 0.15 | 0.98 ± 0.11 | 0.81 ± 0.13 | 0.83 ± 0.07 | 1.01 ± 0.03 | 1.02 |
| $\overline{R}_{B_r}$(HFR4, AST3) | 0.93 ± 0.22 | 1.06 ± 0.13 | 1.07 ± 0.09 | 1.23 ± 0.16 | 1.26 ± 0.07 | 1.06 ± 0.02 | 1.06 |

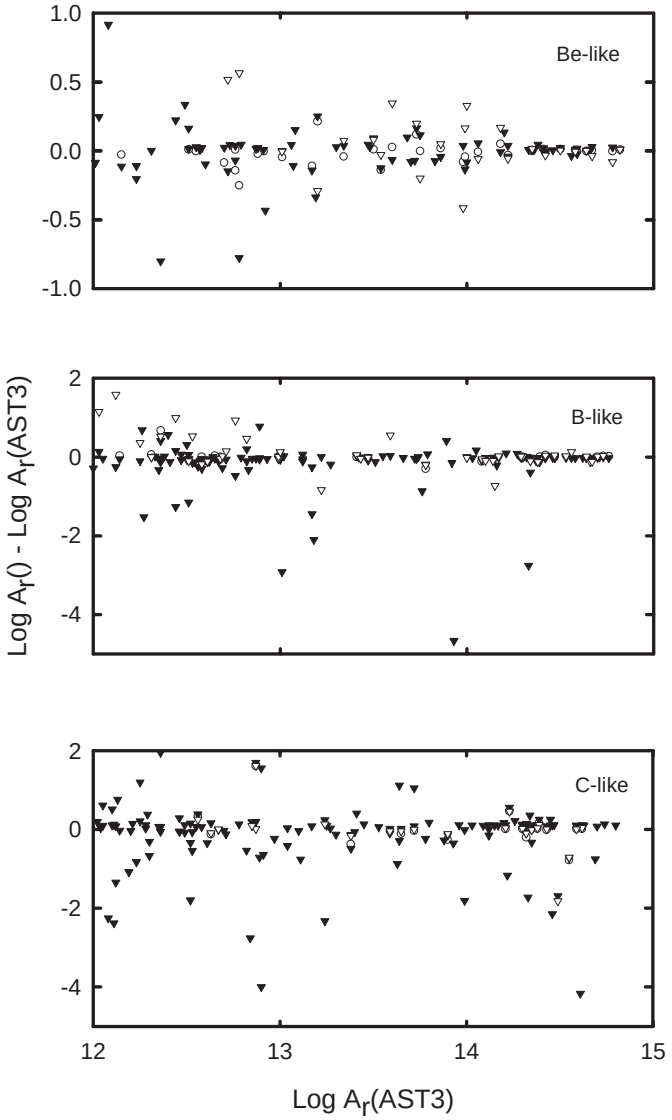


**Fig. 3.** Comparison of $A$-values ($s^{-1}$) computed in approximation AST3 for Fe ions with $4 \leq N \leq 6$ with those in the external data sets COR (circles), SAF (triangles), and MCDF (filled triangles).

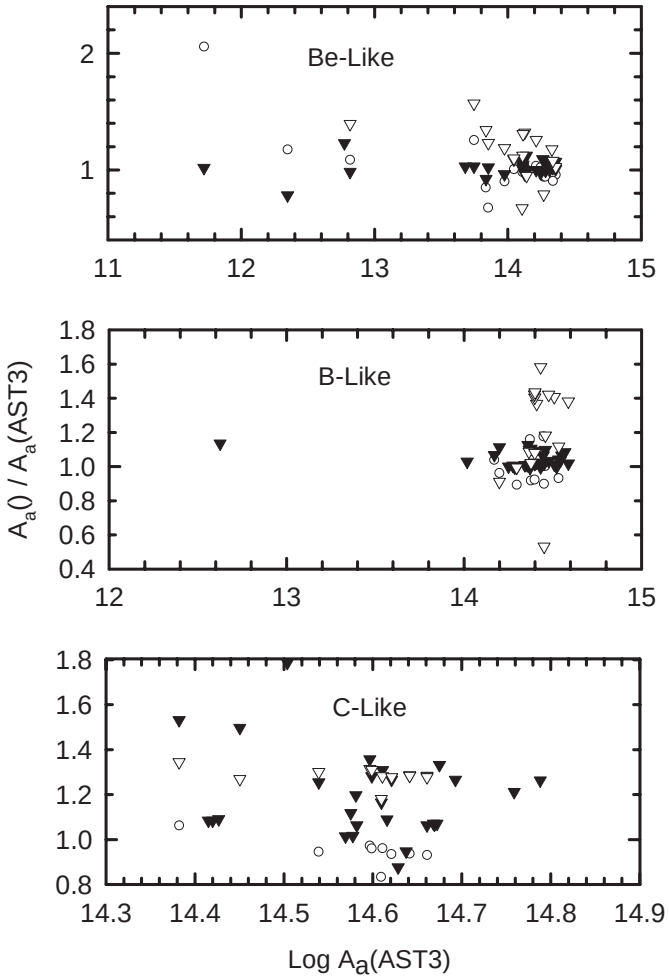


**Fig. 4.** Comparison of total Auger rates ($s^{-1}$) computed in approximations AST3 for Be- through C-like Fe ions with other data sets: COR (circles); SAF (triangles); and MCDF (filled triangles).

the semiempirical corrections have been useful to improve further the accuracy of our data. In this respect, it would have been resourceful to have had more reliable measurements of the strongly coupled and tricky levels of the $1s2s^22p^3$ configuration in Fe XXI and of the questionable solar identifications of the $1s2s^22p^4\ ^2L_J$ and $1s2s^22p^6\ ^2S_{1/2}$ components in Fe XX and Fe XVIII, respectively. They required revised estimates with the laboratory wavelengths by Beiersdorfer et al. (1993) and Decaux et al. (1997) listed in the EXP2 data set. This has not been an easy task since, in spite of the quoted high accuracy, their wavelength data lack the structural consistency that warrants a unique set of spectroscopic level energies. By extensive comparisons with results from the approximations considered, previous calculations and experiment, the statistical accuracy of present level-energy data set has been estimated at better than 3 eV. Our wavelengths and Auger-electron kinetic energies have been derived from the experimental levels when available otherwise from the theoretical values which suggest in the case of the former a statistical accuracy close to ±2 mÅ.

With respect to the $A$-values and partial Auger rates, it has been found that very little can be asserted about transitions with values under $10^{13}$ $s^{-1}$. The accuracy otherwise has been ranked by means of comparisons of several data sets at 20%. Relativistic effects are particularly conspicuous in Fe ions with

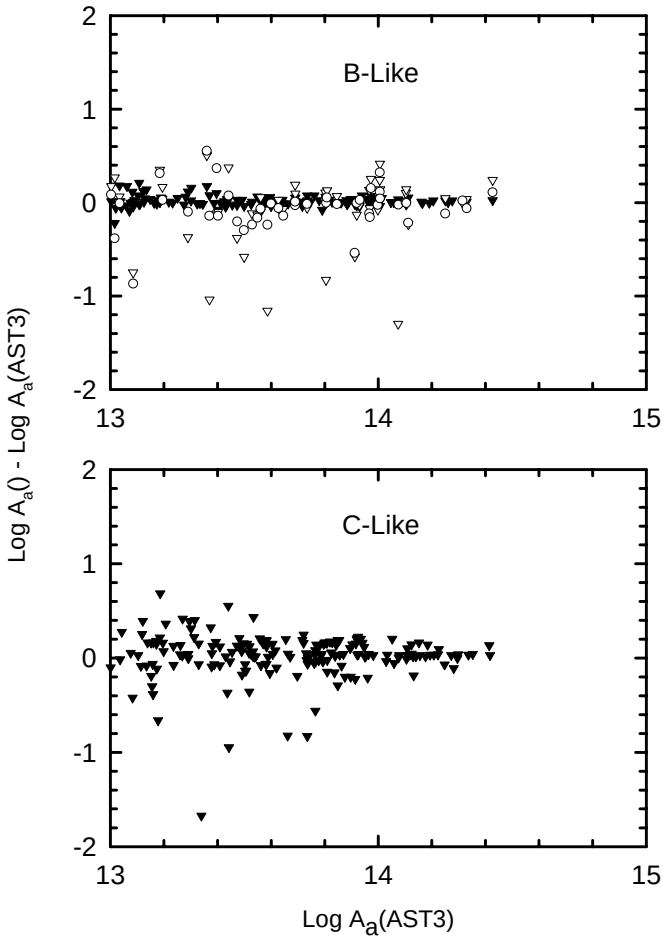


**Fig. 5.** Comparison of partial Auger rates ($s^{-1}$) computed in approximations AST3 for B- through C-like Fe ions with other data sets: COR (circles); SAF (triangles); and MCDF (filled triangles).

$N \leq 4$, but become more manageable for the less ionized species. We are therefore puzzled with the large systematic discrepancies encountered in SAF and MCDF which affect even the large (greater than $10^{14}$ $s^{-1}$) total widths of the higher $N$ systems which in our view can only be attributed to numerical problems. Similarly, while a satisfactory accord is found with the $A$-values in HFR4, we cannot explain the discrepancies encountered in the C-like and N-like ions when the satellite intensity factors and the radiative branching ratios are compared. By contrast the data in COR are in general within the proposed bounds in spite of their neglecting the spin–spin bound-free couplings in the Auger processes.

It has been found that the BPRM and the HFR suites are currently not usable for the calculation of partial Auger rates which are now in demand in the formal modeling of ionization balances and post-Auger radiative emissions. Taking also into consideration their present shortcomings in the representation of the two-body operators of the Breit interaction, our earlier statement about AUTOSTRUCTURE being the platform of choice for inner-shell studies is reaffirmed. We have already made fast progress in tackling the very interesting features of the decay pathways of members of the second row ($10 \leq N \leq 17$) which will be reported elsewhere.

*Acknowledgements.* We are grateful to Dr. Marguerite Cornille, Observatoire de Meudon, France for private communications regarding the approximations made in the COR and SAF data sets, and to Dr. Verne L. Jacobs, Naval Research Laboratory, USA for providing us with printed materials of Table III and IV in Jacobs et al. (1989). CM acknowledges a Senior Research Associateship from the National Research Council, and PP a Research Associateship from University of Maryland. This project is partially supported by FONACIT, Venezuela, through contract No. S1-20011000912.

## References

Badnell, N. R. 1986, J. Phys. B, 19, 3827
Badnell, N. R. 1997, J. Phys. B, 30, 1
Bautista, M., Mendoza, C., Kallman, T. R., et al. 2003, A&A, 403, 339
Becker, S. R., Butler, K., & Zeippen, C. J. 1989, A&A, 221, 375
Beiersdorfer, P., Phillips, T., Jacobs, V. L., et al. 1993, ApJ, 409, 846
Berrington, K. A., Burke, P. G., Butler, K., et al. 1987, J. Phys., B, 20, 6379
Berrington, K. A., Burke, P. G., Chang, J. J., et al. 1974, Comput. Phys. Commun., 8, 149
Berrington, K. A., Burke, P. G., Le Dourneuf, M., et al. 1978, Comput. Phys. Commun., 14, 367
Biémont, E., Frémat, Y., & Quinet, P. 1999, At. Data Nucl. Data Tables, 71, 117
Burke, P. G., Hibbert, A., & Robb, W. D. 1971, J. Phys. B, 4, 153
Burke, P. G., & Seaton, M. J. 1971, Meth. Comp. Phys. 10, 1
Chen, M. H. 1986, At. Data Nucl. Data Tables, 34, 301
Chen, M. H., & Crasemann, B. 1987, At. Data Nucl. Data Tables, 37, 419
Chen, M. H., & Crasemann, B. 1988, At. Data Nucl. Data Tables, 38, 381
Chen, M. H., Reed, K. J., McWilliams, D. M., et al. 1997, At. Data Nucl. Data Tables, 65, 289
Cowan, R. D. 1981, The Theory of Atomic Structure and Spectra (Berkeley, CA: University of California Press)
Decaux, V., Beiersdorfer, P., Kahn, S. M., et al. 1997, ApJ, 482, 1076
Drake, G. W. F. 1986, Phys. Rev. A, 34, 2871
Dubau, J., & Loulergue, M. 1981, Phys. Scr., 23, 136
Eissner, W., Jones, M., & Nussbaumer, H. 1974, Comput. Phys. Commun., 8, 270
Eissner, W., & Nussbaumer, H. 1969, J. Phys. B, 2, 1028
Feldman, U., Doschek, G. A., & Kreplin, R. W. 1980, ApJ, 238, 365
Galavís, M. E., Mendoza, C., & Zeippen, C. J. 1997, A&AS, 123, 159
Galavís, M. E., Mendoza, C., & Zeippen, C. J. 1998, A&AS, 131, 499
Jacobs, V. L., Doschek, G. A., Seely, J. F., et al. 1989, Phys. Rev. A, 39, 2411
Kato, T., Safronova, U. I., Shlyaptseva, A. S., et al. 1997, At. Data Nucl. Data Tables, 67, 225
Mendoza, C., Zeippen, C. J., & Storey, P. J. 1999, A&AS, 135, 159
Quigley, L., & Berrington, K. 1996, J. Phys. B, 29, 4529
Quigley, L., Berrington, K., & Pelan, J. 1998, Comput. Phys. Commun., 114, 225
Safronova, U. I., & Shlyaptseva, A. S. 1996, Phys. Scr., 54, 254
Safronova, U. I., & Shlyaptseva, A. S. 1999, Phys. Scr., 60, 36
Safronova, U. I., Shlyaptseva, A. S., Cornille, M., & Dubau, J. 1998, Phys. Scr., 57, 395
Safronova, U. I., & Urnov, A. M. 1980, J. Phys. B, 13, 869
Scott, N. S., & Burke, P. G. 1980, J. Phys. B, 13, 4299
Scott, N. S., & Taylor, K. T. 1982, Comput. Phys. Commun., 25, 347
Seely, J. F., Feldman, U., & Safronova, U. I. 1986, ApJ, 304, 838
Shapiro, P. R., & Bahcall, J. N. 1981, ApJ, 245, 335
Shirai, T., Sugar, J., Musgrove, A., et al. 2000, J. Phys. Chem. Ref. Data, Monograph 8